AGU ADVANCING EARTH AND SPACE SCIENCES

JGR Atmospheres

Special Section:
Emerging air pollution: emissions, chemistry, and health and climate effects

Key Points:
- MDA8 ozone in summer 2050 will be above WHO guideline of 100 μg/m³ in Beijing–Tianjin–Hebei and Yangtze River Delta under four SSPs
- Vegetative ozone exposure index will be above US secondary standard of 21 ppm-h in Huang–Huai–Hai under SSP370 and SSP585 in summer 2050
- Mortality will mainly reduce by 2050 in four areas under SSPs, but increase in Beijing–Tianjin–Hebei and Yangtze River Delta under SSP245

Supporting Information:
Supporting Information may be found in the online version of this article.

Correspondence to:
Y.-H. Mao,
yhmao@nuist.edu.cn

Future Ozone Changes and Their Impacts on Vegetation and Human Health in China Under the Shared Socio-Economic Pathways

Chen Xu[1], Yu-Hao Mao[1,2] (ID), **and Hong Liao[1,2]** (ID)

[1]Jiangsu Key Laboratory of Atmospheric Environment Monitoring and Pollution Control/Jiangsu Collaborative Innovation Center of Atmospheric Environment and Equipment Technology, School of Environmental Science and Engineering, Nanjing University of Information Science and Technology (NUIST), Nanjing, China, [2]Key Laboratory of Meteorological Disaster, Ministry of Education (KLME)/Collaborative Innovation Center on Forecast and Evaluation of Meteorological Disasters (CIC-FEMD)/International Joint Research Laboratory on Climate and Environment Change (ILCEC), NUIST, Nanjing, China

Abstract Ozone concentrations in China are increasing in recent years and future changes of ozone and their impacts have attracted much attention. We use global chemical transport model (GEOS-Chem) to simulate the surface ozone concentrations in China in 2020 and 2050 under four Shared Socio-economic Pathways and evaluate the impacts of future ozone pollution on vegetation and premature mortality in four polluted regions (Beijing–Tianjin–Hebei, BTH; Yangtze River Delta, YRD; Pearl River Delta, PRD; Sichuan Basin, SCB) and three major crop growing areas (Huang–Huai–Hai, HHH; Northeast Plain, NEP; middle and lower reaches of Yangtze River, MLRY) in China. The changes of simulated seasonal maximum daily 8-hr average (MDA8) ozone from 2020 to 2050 (−15.5 to +11.9 ppbv) are significant under SSP126 (low forcing pathway) and SSP245 (medium forcing pathway) scenarios in all regions due to large changes of emissions. MDA8 ozone in summer 2050 will be above the WHO guidelines (100 μg/m³) in BTH, YRD, HHH and MLRY under four scenarios. By 2050, W126 (vegetative ozone exposure index) in summer will be much above the maximum of US secondary standard (21 ppm-h) in HHH under SSP245, SSP370 (medium to high forcing pathway) and SSP585 (high forcing pathway) scenarios, and in MLRY under SSP370 and SSP585 scenarios. Annual ozone-related deaths for people over 30 years old will mainly decrease in four polluted areas from 2020 to 2050 under SSPs scenarios, but only increase much under SSP245 scenario in BTH (+3.1 to +4.2 thousand) and YRD (+1.1 to +1.6 thousand).

Plain Language Summary With the development of industrialization and urbanization, ozone pollution in China has become increasingly serious. Ozone pollution is harmful to vegetation and human health and thus future ozone in China and its impacts have attracted much attention. We use global chemical transport model to simulate ozone concentrations in 2020 and 2050 under four emission scenarios and then quantify the effects of future ozone pollution on premature mortality and vegetation in four polluted regions and three major crop growing areas in China. Seasonal MDA8 ozone concentrations and vegetative ozone exposure index (W126) change much from 2020 to 2050 under low and medium forcing pathways due to large changes of emissions. Due to ozone pollution, vegetation in summer 2050 will be at high risk in Huang–Huai–Hai region under medium to high and high forcing pathways. Ozone-related deaths will mainly decrease under future emission scenarios in four polluted areas by 2050, but increase much under medium forcing pathway in Beijing–Tianjin–Hebei and Yangtze River Delta regions.

1. Introduction

Surface ozone is mainly generated by precursors (including VOCs and NOx) through photochemical reactions under sunlight (Wang et al., 2017), which has serious effects on human health (Alexis & Carlsten, 2014; Goodman et al., 2015; Sousa et al., 2013), ecosystems (Emberson, 2020; Grulke & Heath, 2019; Ren, Tian, Chen, et al., 2007, Ren, Tian, Liu, et al., 2007, 2011), and crop yields (Bhatia et al., 2012; Feng et al., 2015). With the development of industrialization and urbanization, ozone pollution in China has become increasingly serious (Mousavinezhad et al., 2021). Although the Chinese government implemented stricter measures to control pollutant discharge after 2013, Report on the Ministry of Ecology and Environment of China (https://www.mee.gov.cn/hjzl/sthjzk/zghjzkgb/) showed that annual average ozone concentrations had a fluctuating upward

trend from 2013 (139 μg/m^3) to 2019 (148 μg/m^3). Because of the current high level of ozone pollution in China, the future ozone in China and its impacts on vegetation growth and human health have attracted much attention.

Shared Socio-economic Pathways (SSPs) scenarios describe future possible evolution of population, economy, policies and institutions, technology, and environment and natural systems in the 21st century (O'Neill et al., 2017). Based on SSPs scenarios, studies have predicted future ozone concentrations in China, which will be mainly affected by changes in climate and anthropogenic emissions (Liu et al., 2021; Liu et al., 2022). The reductions of MDA8 ozone caused by emission reductions associated with sustainable development (difference between SSP126 scenario and SSP585 scenario) would range from 7.5% to 25.3% in China in 2050, which would be more than 10 times greater than that caused by climate changes (Liu et al., 2021). Liu et al. (2022) studied the sensitivity of ozone to emission changes from the current (2004–2014) to the future (2045–2055) and found that ozone concentrations would increase both in winter and summer in the eastern China under SSP370-lowNTCF (near-term climate forcers) scenario and increase in summer but decrease in winter in East Asia under SSP370 scenario.

Exposure to high concentrations of ozone can cause diseases of human respiratory system, cardiovascular system, and nervous system (Jerrett et al., 2009). The Global Burden of Diseases, Injuries, and Risk Factors Study 2015 reported that environmental ozone exposure was the 34th risk factor out of 79 for global mortality (Cohen et al., 2017). Ozone-related deaths accounted for about 8.0% of chronic obstructive pulmonary disease (COPD) deaths globally in 2015, with the highest ozone-related deaths in China and India (Cohen et al., 2017). Changes in climate, emissions, and population will affect the ozone pollution and thus human health in the future (Chen et al., 2018; Hong et al., 2019; Liu et al., 2021; Wang, Hu, et al., 2021). Studies have shown that changes in emissions will have the major impact on the ozone-related mortality changes in most regions of China (Liu et al., 2021; Wang, Hu, et al., 2021). By using GFDL-CM3, Chen et al. (2018) found that annual ozone-related mortality would decrease by 24% in 2050s relative to 2013–2015, due to the decrease of ozone precursor emissions under representative concentration pathway RCP4.5 scenario. For RCP8.5 scenario, climate warming and high emissions would lead to an increase of 10.7% in mortality (Chen et al., 2018). Combined WRF-CMAQ and SSPs scenarios, Liu et al. (2021) showed that the changes of ozone-related mortality caused by emission reductions associated with sustainable development would be approximately 2 orders of magnitude larger than those caused by meteorological changes in China by 2050. Based on GEOS-Chem, Wang, Hu, et al. (2021) found that the decrease of ozone concentrations would avoid 30.2% (18.0%) related mortality under RCP2.6 (RCP4.5) scenario from 2010 to 2050, but the increase of population size only led to a slight increase in ozone-related mortality.

Ozone is a phytotoxic pollutant, which enters leaves through stomata, produces oxidizing substances and affects physiological and biochemical processes (Grulke & Heath, 2019), thereby causes visible injuries to leaves, germination delay (Grulke & Heath, 2019; Ren, Tian, Chen, et al., 2007) and crop yield reduction (Wang et al., 2017). Model-based simulations can predict the impact of ozone exposure on vegetation in future. Based on Community Earth System Model (CESM), Tai et al. (2014) found that ozone pollution control could greatly increase wheat yield in China under RCP4.5 scenario during 2020–2050, and severe ozone pollution would reduce total global crop production by 3.6% under RCP8.5 scenario. Combined CESM and the partial derivative-linear regression model, Tai and Val Martin (2017) projected that wheat, corn, and soybean yields in China would decline by 7.7%, 0.91% and 5.2% by 2050 under RCP8.5 scenario just because of the increase in ozone.

Some indexes are often used to assess the effect of ozone exposure to vegetation. Among them, W126 is a biologically related cumulative and seasonal index (EPA, 2015), which reflects the harm of different concentrations of ozone to vegetation. Based on W126 calculated by WRF-CMAQ simulation results, Qiao et al. (2019) found that W126 with area-weighted mean was 37.6 ppm-h across China and ozone exposure could cause foliar injuries of highly sensitive species in 100% of forest region in 2013. In China, W126 of April–September calculated by 243 observation stations increased by 16.3% annually from 2013 to 2019 (Lu et al., 2020) and monthly averaged W126 of 1,497 stations exceeded the standard level (7–21 ppm-h) by 1.2 times for 2015–2016 (Li et al., 2018). The observed W126 were 17.1–54.2 ppm-h in Sichuan Basin cities (Cao et al., 2020) in 2018 and 29.0 ppm-h in Yancheng (Wang et al., 2020) in 2019, which all far exceeded the minimum of US standard level (7 ppm-h). The W126 from April to September for 2018−2020 reduced by 28.6%, 9.8%, 6.7% and 23.1%, respectively, in Pearl River Delta, Yangtze River Delta, Chengdu-Chongqing and Fen Wei Plain because of the reduction of ozone for Three-year Action Plan on ozone pollution (Zhao et al., 2022).

As far as we know, there is a lack of systematic evaluation for effects of ozone on future vegetation and human health in different polluted regions and major crop growing areas of China. In this study, we use global chemical transport model (GEOS-Chem) to predict the characteristics of ozone concentrations in 2050 under four different emissions scenarios (SSP126, SSP245, SSP370, and SSP585 scenarios) and then further evaluate the effects of future ozone pollution on premature mortality and vegetation in four polluted regions and three major crop growing areas of China. Section 2 describes the GEOS-Chem model and indexes of ozone impacts on vegetation and human health. Section 3 evaluates model results with observed ozone concentrations in 2015 and 2020 across China. In Section 4, changes of ozone concentrations between 2050 and 2020 under four emissions scenarios are shown. In Sections 5 and 6, we evaluate the changes of vegetation and human health due to ozone exposure in 2020 and 2050 by using W126 and premature mortality. Finally, we draw conclusions and discuss the uncertainties and future work in Section 7.

2. Data and Methods

2.1. Model

We use in this study the chemical transport model GEOS-Chem (v12-09, https://wiki.seas.harvard.edu/geos-chem/index.php/GEOS-Chem_12#12.9.2) (The International GEOS-Chem User Community, 2020) with global simulations at a horizontal resolution of 2° latitude by 2.5° longitude. The vertical resolution is set to 47 layers, extending up to 0.1 hPa. Model simulations are driven by MERRA2 reanalyzed data from Goddard Earth Observing System (GEOS) of the NASA Global Modeling and Assimilation Office (GMAO). We fix the MERRA2 meteorological field in the year 2020 and simulate hourly ozone concentrations in China in 2020 and 2050 to investigate future changes of ozone concentrations due to changes of anthropogenic and open-burning emissions and their impacts on vegetation and human health. All simulations are spin up for 6 months in each year.

The GEOS-Chem model includes the tropospheric chemical mechanism of "NOx-O_3-HC-aerosol" (Wang et al., 1998). NASA Jet Propulsion Laboratory and International Union of Pure and Applied Chemistry (IUPAC) provide chemical kinetics data for model simulation (Sander et al., 2011). Fast-JX scheme is used to calculate the light reaction rate in the model (Bian & Prather, 2002). The parameterization scheme of dry deposition of gas and aerosol (except sea salt) is based on online resistance-in-series model (Wesely, 1989; Zhang et al., 2001) and wet deposition of water-soluble aerosols and gases is described by Liu et al. (2001) and Amos et al. (2012). Lin and McElroy. (2010) provide a non-local scheme for boundary layer mixing process. Holmes et al. (2019) and McDuffie et al. (2018) have updated the mechanism of heterogeneous reaction and cloud chemistry.

2.2. Emissions

In this study, we use future emissions SSPs Tier-1 scenarios at 0.5° × 0.5° resolution for model simulations. Tier-1 scenarios include SSP126, SSP245, SSP370, and SSP585 and are designed to provide full-range forced targets similar in magnitude and distribution to the RCPs used in Coupled Model Intercomparison Project Phase 5 (CMIP5) (Gidden et al., 2019). SSP126, SSP245, SSP370, and SSP585 scenarios represent low, medium, medium to high, and high future forcing pathways, respectively. These four SSP-based scenarios cover a wide range of uncertainty for climate science studies about future forcing pathways (O'Neill et al., 2016). The year 2015 is the transition year in CMIP6 between historic and future simulations, and the emissions in 2015 are the same under four SSPs scenarios (Gidden et al., 2019). In the present study, we use the emissions for the year 2020 to represent present-day pollution level and compare the changes between 2020 and 2050. Monthly anthropogenic and open-burning emission data of the SSP126, SSP245, SSP370, and SSP585 scenarios at 2015, 2020, and 2050 can be downloaded at https://esgf-node.llnl.gov/search/input4MIPs/. Open-burning emissions are only about or less than 1% of anthropogenic emissions in China.

Figure 1 shows the annual total anthropogenic emissions of NOx, CO, CH_4, and NMVOCs in China in 2020, 2030, 2040, and 2050 under SSP126, SSP245, SSP370, and SSP585 scenarios. Seasonal and annual anthropogenic emissions of NOx and NMVOCs in seven study areas in China (shown in Figure 2) in 2020 and 2050 under four SSPs scenarios and the corresponding percentage changes for 2020–2050 are shown in Tables S1 and S2 in Supporting Information S1. The emissions of four species in 2050 are lowest under SSP126 scenario and highest under SSP370 scenario. Compared to other lower forcing pathways, the SSP585 scenario, classified as high future forcing pathway, shows medium emissions for the four species, as SSP5 scenario models a future world driven by
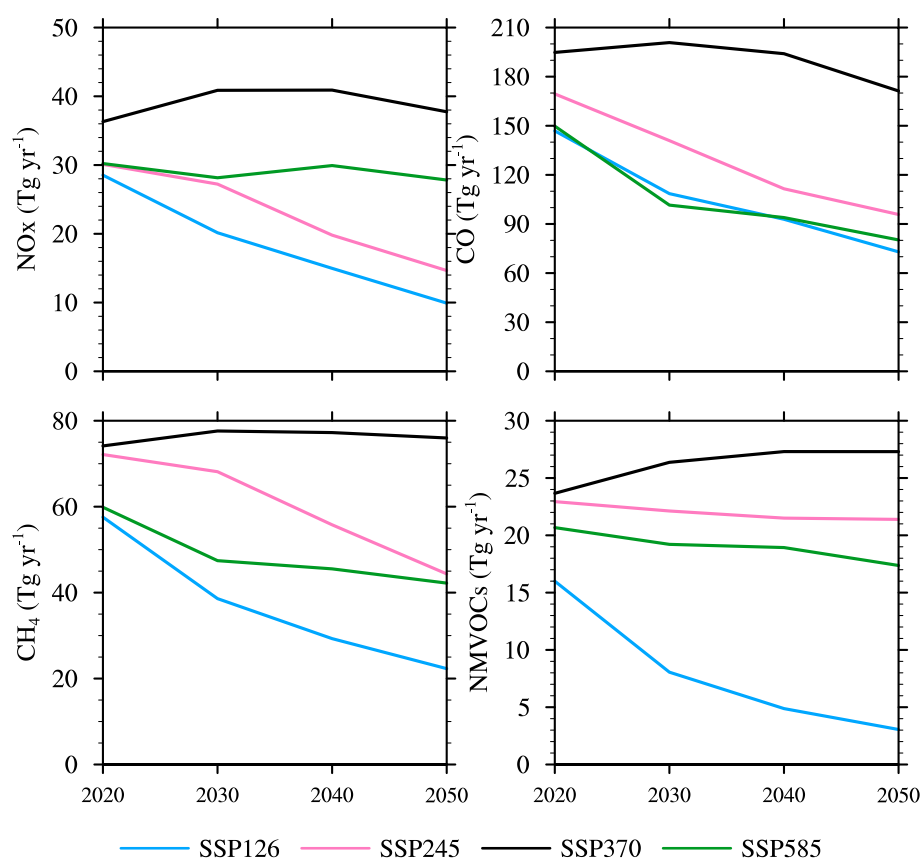
Figure 1. Total annual anthropogenic emissions of nitrogen oxides (NOx), carbon monoxide (CO), methane (CH$_4$), and non-methane volatile organic compounds (NMVOCs) in China for 2020, 2030, 2040, and 2050 under SSP126, SSP245, SSP370, and SSP585 scenarios.

the fossil-fuel and with the highest CO$_2$ emission (Gidden et al., 2019). Under SSP126 (SSP245) scenario, the emissions of NOx, CO, CH$_4$, and NMVOCs show a decreasing trend for 2020–2050, with the reductions of 65.3% (51.3%), 50.3% (43.6%), 61.3% (38.5%) and 80.9% (6.7%), respectively. For SSP370 scenario, the emissions of NOx, CO, CH$_4$, and NMVOCs are higher than their respective emissions under SSP126, SSP245, and SSP585 scenarios during 2020–2050, especially for the emissions of CO and CH$_4$ after 2030. The SSP370 scenario shows peaks at 2030 for CH$_4$ (77.6 Tg) and CO (200.8 Tg) and at 2040 for NOx (40.9 Tg). NMVOCs emissions under SSP370 scenario increase by 15.2% from 2020 to 2050. Under SSP585 scenario, NOx emissions show a downward trend for 2020–2030, increase slightly during 2030–2040, reach a peak value of 29.9 Tg in 2040 and then decline after 2040. Emissions decrease continuously from 2020 to 2050 for CO, CH$_4$, and NMVOCs under SSP585 scenario, with the reductions of 69.5 Tg (46.4%), 17.7 Tg (29.5%) and 3.3 Tg (16.0%), respectively.

Natural emissions used in the model simulations are the same for 2020 and 2050, representing the current emission levels. Biological NMVOC emissions are calculated using the module of Natural Gas and Aerosol emission Model (MEGAN) (Guenther et al., 2012). BVOCs emitted by vegetation will be affected if vegetation is damaged by future ozone (Hollaway et al., 2017), but which is not reflected in the current model simulation (Guenther et al., 2012). Sauvage et al. (2007) and Murray et al. (2012) describe NOx emissions from lightning. Soil NOx emissions are calculated using the algorithm proposed by Yienger and Levy Ii (1995).

2.3. W126 (Seasonal Vegetative Ozone Exposure Index)

We use W126 to quantify the impact of ozone cumulative exposure on vegetation. Based on evidence that plant stomatal conductance, ozone concentrations and uptake rates increase to a diurnal peak during the daytime (Uddling et al., 2010), W126 ozone index is generally calculated as the sum of sigmoidally-shaped weighted hourly ozone concentrations during the daytime (8:00–20:00 local time) (EPA, 2015):
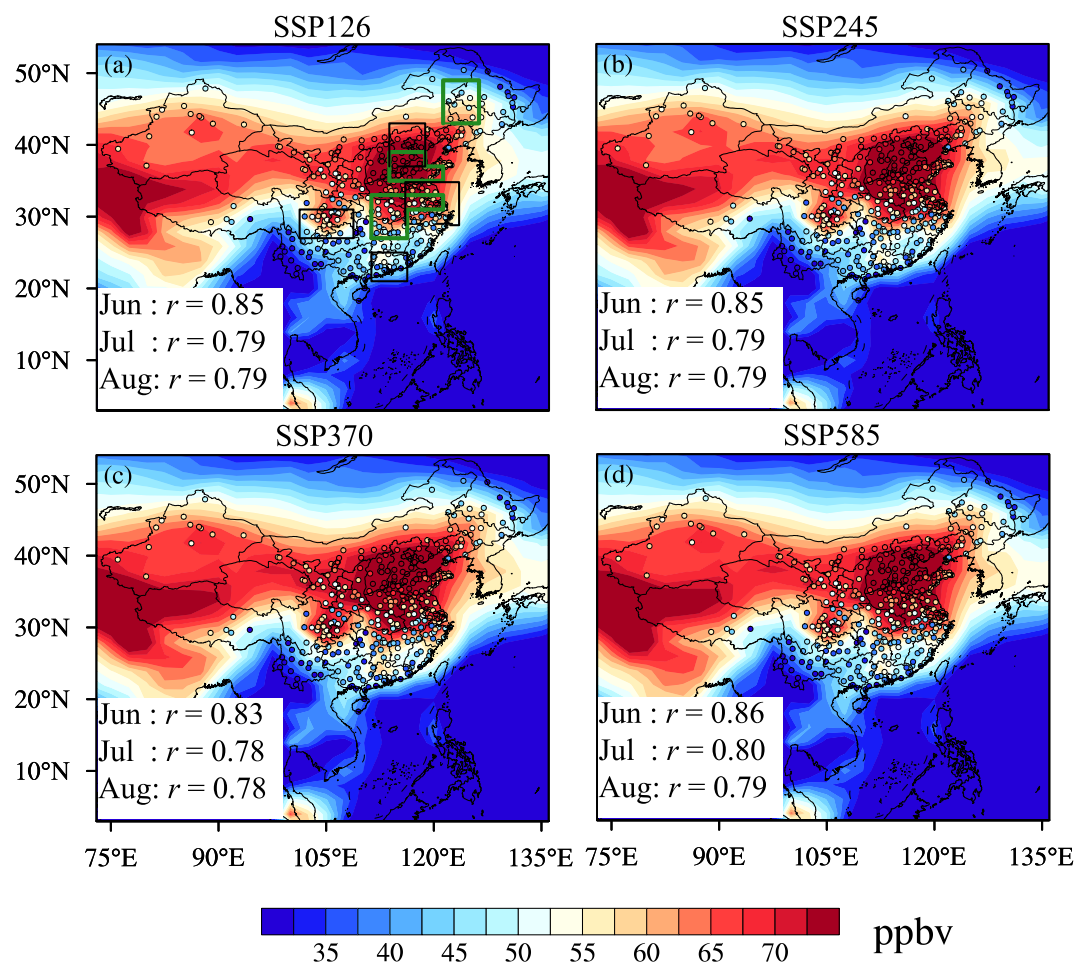
Figure 2. Observed and simulated spatial distributions of MDA8 ozone concentrations averaged for summer (June–July–August) 2020 under (a) SSP126, (b) SSP245, (c) SSP370, and (d) SSP585 scenarios. Colored dots represent the observations in summer 2020 averaged for all sites in every city. Four polluted regions are highlighted by black rectangles: Beijing–Tianjin–Hebei (BTH, 37°–43°N, 113.75°–118.75°E), Yangtze River Delta (YRD, 29°–35°N, 116.25°–123.75°E), Pearl River Delta (PRD, 21°–25°N, 111.25°–116.25°E), and Sichuan Basin (SCB, 27°–31°N, 101.25°–108.75°E). Three major crop growing areas are highlighted by green rectangles: Huang–Huai–Hai area (HHH, 35°–39°N, 113.75°–118.75°E and 35°–37°N, 118.75°–121.25°E), Northeast Plain area (NEP, 43°–49°N, 121.25°–126.25°E), and the middle and lower reaches of the Yangtze River (MLRY, 27°–33°N, 111.25°–116.25°E and 31°–33°N, 116.25°–121.25°E).

$$W126 = \sum_i w_i \times C_i \qquad (1)$$

$$w_i = \frac{1}{[1 + 4403 \cdot \exp(-126 \cdot C_i/1000)]} \qquad (2)$$

where C_i is the hourly ozone concentration in ppbv. w_i is weighted index, w_i emphasizes high ozone concentrations while suppresses low or moderate ozone concentrations, such as 0.06 at 45 ppbv and 0.7 at 75 ppbv. Monthly W126 is calculated by adding up the daily W126 in a given month (EPA, 2015; Lapina et al., 2014). In this paper, we use simulated hourly ozone to calculate the sum of monthly W126 for spring (March, April and May), summer (June, July and August), autumn (September, October and November), and winter (December, January and February) and then analyze the seasonal variation of W126 over a year. The United States Environmental Protection Agency (EPA) currently recommends a 3-month W126 value of 7–21 ppm-h (ppm-hours, sigmoidal-weighted cumulative exposure for daytime) (Marco et al., 2020) as a secondary standard for assessing the risk of ozone exposure to vegetation.

2.4. Health Impact Assessment of Ozone Exposures

The premature mortalities in adults older than 30 years of age attributable to ozone exposure are calculated according to the following equation from Jerrett et al. (2009) and Turner et al. (2016):

$$\Delta \text{Mort} = \sum_{i=1}^{n} pop_i * y_0 * \frac{\text{RR}_{i,j} - 1}{\text{RR}_{i,j}} \tag{3}$$

$$\text{RR}_{i,j} = \exp(\beta * (X - X_0)) \tag{4}$$

$$\beta = ln^{\text{HR}} / \Delta \text{Y} \tag{5}$$

where ΔMort is premature mortality caused by ozone due to different disease categories j, including cardiovascular disease (CVD), respiratory diseases (RD), and chronic obstructive pulmonary disease (COPD) in this study. pop_i is the population older than 30 years of age for grid i. Population changes under four SSPs scenarios from 2020 to 2050 is shown in Table S3 in Supporting Information S1. Gridded population in 2020 and 2050 under four SSPs scenarios is from http://sedac.ciesin.columbia.edu/data/set/popdynamics-1-8th-pop-base-year-projection-ssp-2000-2100-rev01/data-download (Jones & O'Neill, 2020). The percentage of population over 30 years old is achieved from the United Nations estimates (https://population.un.org/wpp/Download/Standard/Population/) (United Nations, 2019). y_0 is the baseline mortality of the particular disease category. The y_0 older than 30 years of age is 0.0046, 0.0011, and 0.00105 for CVD, RD, and COPD, respectively, which is calculated based on data from Global Health Estimates 2019 by World Health Organization (WHO) (https://www.who.int/data/global-health-estimates) (WHO, 2020) and following the approach by Dang and Liao (2019).

$\text{RR}_{i,j}$ is the relative risk for disease j at grid i caused by ozone, which is calculated by the log-linear exposure-response function by Jerrett et al. (2009). β is referred to as the concentration response function to estimate the association of ozone concentrations and mortality of particular disease (Malley et al., 2017; Sun et al., 2021; Wang, Hu, et al., 2021). HR is the hazard ratio, which represents the increase in death under 10-ppb rise in long-term ozone exposure (Malley et al., 2017; Turner et al., 2016). ΔY is the increase of ozone concentrations and assumed to 10 ppb in Equation 5. X is the annual average MDA8 ozone and X_0 is the threshold concentration of 26.7 ppb representing minimum ozone exposure from the study of Turner et al. (2016). We use simulated ozone concentrations to calculate annual premature mortality of CVD, RD, and COPD in 2020 and 2050 under four scenarios.

3. Model Evaluation

Previous studies (Dang et al., 2021; Lou et al., 2015; Lu et al., 2019; Ni et al., 2018; Zhu et al., 2017) have shown that GEOS-Chem model could well simulate the temporal and spatial distributions of ozone concentrations in China. We use hourly observations from 1,652 stations in 2020 and 934 stations in 2015 released by the China National Environmental Monitoring Center (https://quotsoft.net/air/) (CNEMC, 2023) to evaluate the performance of ozone simulations in GEOS-Chem under different emission scenarios. Figure 2 shows the spatial distributions of observed and simulated MDA8 ozone concentrations averaged for summer (June–July–August) 2020 under SSP126, SSP245, SSP370, and SSP585 scenarios. The colored dots represent the observed concentrations in summer 2020 averaged for all sites in every city.

The spatial distributions of seasonal mean ozone concentrations simulated under SSP126, SSP245, SSP370, and SSP585 scenarios are similar in summer 2020 and successfully reproduce the spatial distribution characteristics of observed ozone. Model reasonably reproduces the observed MDA8 ozone concentrations in Southwest China, Loess Plateau, North China Plain and northern Northeast Plain, where the differences of simulated and observed MDA8 ozone concentrations are within 2 ppbv in summer under four scenarios. Model results generally overestimate observed MDA8 ozone concentrations over eastern Himalaya, eastern Sichuan Basin, and central China under SSP126, SSP245, and SSP585 scenarios (difference of simulated and observed MDA8 ozone concentrations larger than 15 ppbv), while underestimate in lower reaches of the Yellow River. Simulated results are generally higher under SSP370 scenario than under the other three scenarios due to higher anthropogenic emissions, significantly over northwestern China, Sichuan Basin, central China, and northern Northeast Plain.

We use the correlation coefficient (r), normalized mean biases (NMB), mean fractional bias (MFB) and mean fractional error (MFE) to further assess the performance of model simulation results. We compare the observed monthly mean MDA8 ozone concentrations for each site and the simulated results sampled at the corresponding location of the site to evaluate the model performance.

$$r = \frac{\sum_{i=1}^{N}(c_{m_i} - \overline{c_m})(c_{o_i} - \overline{c_o})}{\sqrt{\sum_{i=1}^{N}(c_{m_i} - \overline{c_m})}\sqrt{\sum_{i=1}^{N}(c_{o_i} - \overline{c_o})}} \tag{6}$$

$$NMB = \left[\sum_{i=1}^{N}(C_{mi} - C_{oi})\right] \Bigg/ \left(\sum_{i=1}^{N} C_{oi}\right) \tag{7}$$

$$MFB = \frac{1}{N}\sum_{i=1}^{N}\frac{c_{m_i} - c_{o_i}}{(c_{m_i} + c_{o_i})/2} \tag{8}$$

$$MFE = \frac{1}{N}\sum_{i=1}^{N}\frac{|c_{m_i} - c_{o_i}|}{(c_{m_i} + c_{o_i})/2} \tag{9}$$

where C_m and C_o are the simulated and observed monthly mean ozone MDA8 concentrations in each observation site, respectively.

GEOS-Chem model generally captures the observed monthly mean MDA8 ozone concentrations in 2020 with the r (NMB) values of 0.76 (0.86%), 0.77 (4.58%), 0.74 (3.19%) and 0.77 (4.52%) under SSP126, SSP245, SSP370, and SSP585 scenarios, respectively. In JJA, the corresponding r between simulations and observations are up to 0.81, 0.81, 0.80 and 0.82, and NMB are 13.29%, 16.54%, 19.64% and 16.83%, respectively. According to the study by Boylan and Russell (2006), the performance of GEOS-Chem for MDA8 ozone simulations is within the model performance goals, with the MFB less than ± 30% (11.31%–21.59%) and MFE less than 50% (16.28%–22.64%). Our simulated results are generally accepted under different emission scenarios and consistent with the GEOS-Chem model study by Zhu and Liao (2016), but with higher correlation coefficient of simulated and observed ozone. We also assess the performance of GEOS-Chem in 2015 when all emissions are the same under four scenarios, and the r and NMB values are 0.71 and −46.42%, respectively. The discrepancy between observed and simulated results may result from model resolutions, chemical mechanisms, meteorology and emissions scenarios. Chemical mechanisms can lead to large uncertainties in the prediction of ozone concentrations (Knote et al., 2015; Mar et al., 2016; Weng et al., 2023). For example, the model studies by WRF-Chem show that ozone concentrations under MOZART mechanism are higher than those under CBMZ mechanism in China in summer 2030 (Weng et al., 2023) and those under RADM2 mechanism over Europe in summer 2007 (Mar et al., 2016).

4. Ozone Concentrations in China in 2020 and 2050

We further study the seasonal mean MDA8 ozone concentrations in 2020 and 2050 under SSP126, SSP245, SSP370, and SSP585 scenarios over four highly populated and polluted regions (BTH, Beijing–Tianjin–Hebei; YRD, Yangtze River Delta; PRD, Pearl River Delta; and SCB, Sichuan Basin) in China (Xu et al., 2022) and three major crop growing areas (HHH, Huang–Huai–Hai area; NEP, Northeast Plain area; and MLRY, the middle and lower reaches of the Yangtze River) according to the major agricultural regions classified by Xia et al. (2018) (Figures 3a and 4a). Figures 3b and 4b show the changes of seasonal mean MDA8 ozone from 2020 to 2050 in BTH, YRD, PRD, SCB, HHH, NEP and MLRY under four scenarios. High concentrations of ozone exposure may adversely affect crop yields (Ren, Tian, Liu, et al., 2007) in three major crop growing areas. The WHO Global Air Quality Guidelines provide recommendations on air quality guideline levels and interim targets with 100 μg/m³, that is, ~51 ppbv for 8-hr average ozone (short-term exposure) (https://www.who.int/publications/i/item/9789240034228).

The seasonal variation characteristics of ozone are quite close over BTH, YRD, HHH and MLRY. Seasonal ozone concentrations are highest in summer under the four scenarios in 2020 and in 2050, but lowest in winter. Changes
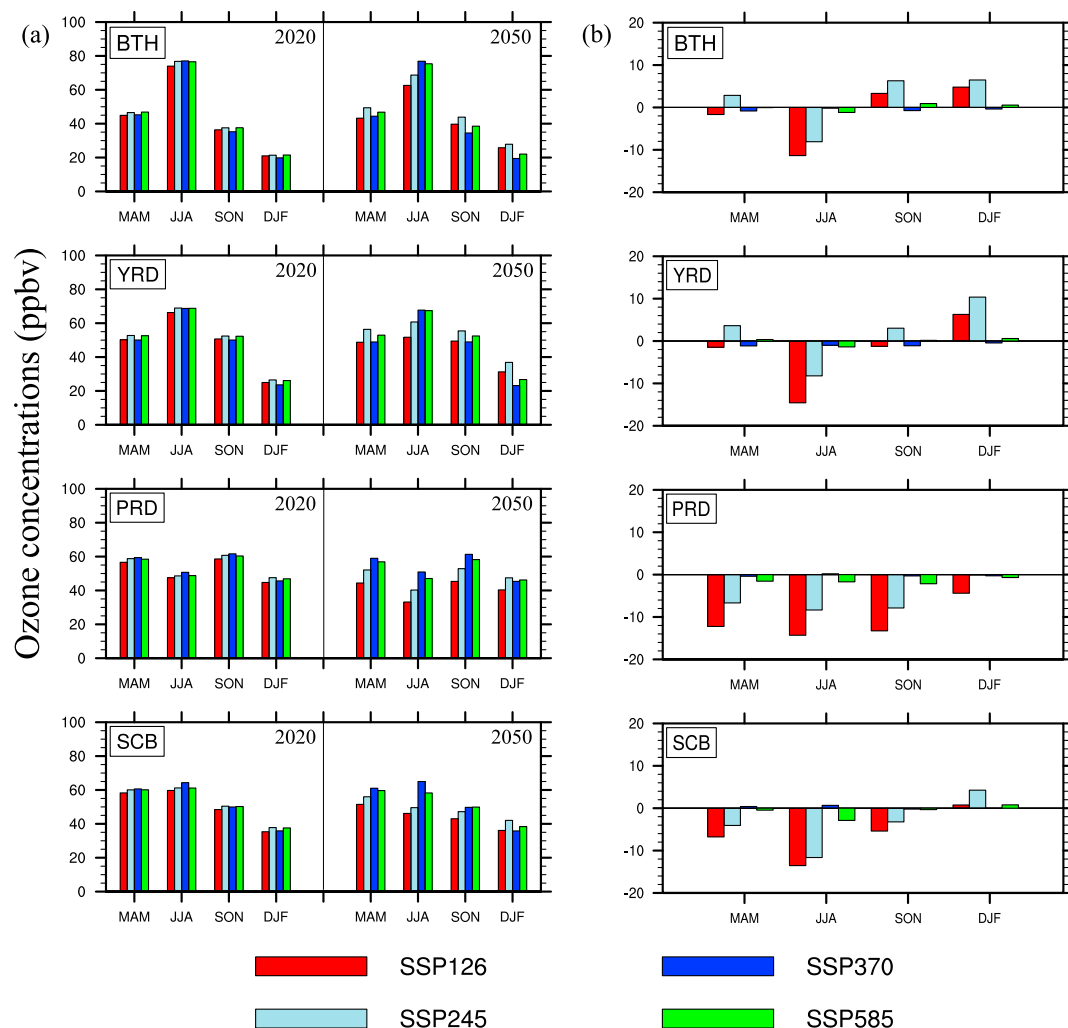
Figure 3. (a) Seasonal mean MDA8 ozone concentrations (ppbv) in 2020 and 2050 and (b) differences of seasonal mean MDA8 ozone concentrations (ppbv) between 2050 and 2020 in Beijing–Tianjin–Hebei region, Yangtze River Delta, Pearl River Delta, and Sichuan Basin under SSP126, SSP245, SSP370, and SSP585 scenarios.

of ozone concentrations from 2020 to 2050 are slight for four seasons under SSP370 (−1.2 to +0.02 ppbv) and SSP585 (−2.1 to +2.3 ppbv) scenarios in these four areas (Figures 3b and 4b). However, changes are great under SSP126 (SSP245) scenario in summer and winter, especially reaching −15.5 (−12.0) ppbv in MLRY in summer. Great anthropogenic emission reductions of ozone precursors occur in summer from 2020 to 2050 under SSP126 and SSP245 scenarios, leading to the decrease of ozone concentrations (Tables S2 and S3 in Supporting Information S1, Liu et al., 2022). For these four areas, the small rise of ozone concentrations under SSP126 and SSP245 scenarios in winter is probably caused by the significantly projected reduction in NOx emissions at low VOCs/NOx ratio from 2020 to 2050. By 2050, SSP370 scenario will be the worst for ozone concentrations in summer in four regions compared to other scenarios. In 2050, the summer MDA8 ozone concentrations in the four regions are all above the WHO guideline under the four scenarios. Meanwhile, MDA8 ozone is higher than WHO guideline in HHH (MLRY and YRD) under SSP245 scenario (SSP245, SSP370 and SSP585 scenarios, and SSP245 and SSP585 scenarios) in spring and in YRD (MLRY) under SSP245 and SSP585 scenarios (SSP245 scenario) in autumn. The public health is likely to suffer ozone pollution in these situations by 2050.

For PRD, MDA8 ozone concentrations in 2020 are high in spring and autumn (58.3 and 60.3 ppbv averaged over four scenarios), but low in summer and winter (48.9 and 46.2 ppbv) (Figure 3a). The occurrence of surface high pressure ridges and tropical cyclones generally leads to low wind speeds and increases ozone concentrations in autumn (Hu et al., 2021; Wang et al., 2009; Zheng et al., 2010; Zhu & Liao, 2016). MDA8 ozone is low during
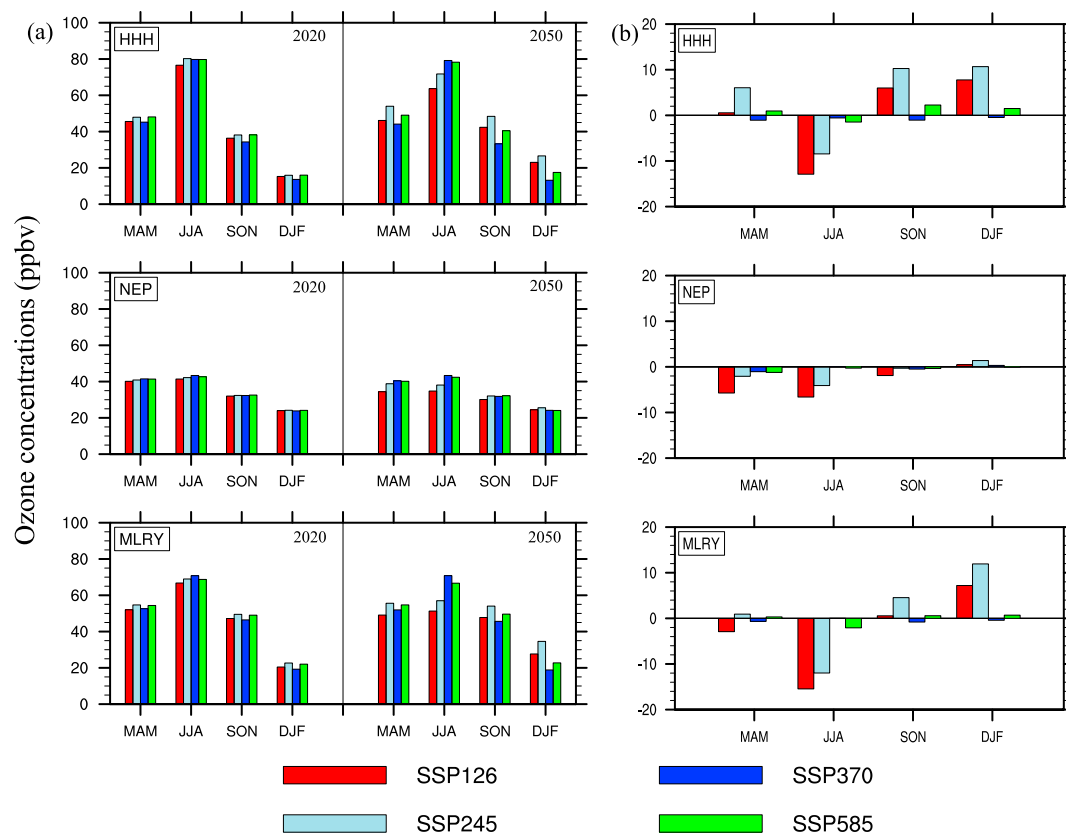
Figure 4. Same as Figure 3, but for Huang–Huai–Hai area, Northeast Plain area, and the middle and lower reaches of the Yangtze River.

summer mainly associated with south or south-west monsoon bringing clean oceanic air which thus decreases ozone concentrations (Wang et al., 2009; Wang, Shen, et al., 2021; Zheng et al., 2010). By 2050, MDA8 ozone concentrations in spring, summer, and autumn are all the highest under SSP370 scenario compared with the other scenarios, reaching 59.0, 50.9 and 61.3 ppbv, respectively, and the highest ozone in winter is 47.5 ppbv under SSP245 scenario. MDA8 ozone in PRD in 2050 is still higher than the WHO guideline in spring and autumn under SSP245, SSP370, and SSP585 scenarios. Ozone concentrations show a consistent downward trend under four scenarios in all seasons from 2020 to 2050, especially under SSP126 scenario. Under SSP126 (SSP245) scenario, seasonal mean ozone decreases by 4.4–14.3 (0.08–8.4) ppbv from 2020 to 2050 due to the large reductions of NOx and NMVOCs anthropogenic emissions. For SSP370 (SSP585) scenario, seasonal mean ozone concentrations change slightly from 2020 to 2050, with the changes of −0.4 to +0.2 (−2.2 to −0.7) ppbv in four seasons.

In SCB, MDA8 ozone concentrations are high in spring and summer but low in autumn and winter (Figure 3a). Ozone pollution happens in SCB mainly owing to the high precursor emissions, the complex basin terrain and frequent stagnant conditions (Sun et al., 2021; Yang et al., 2020). SCB exhibiting high MDA8 ozone levels in spring may result from local emission and transport of ozone affected by changes in the wind fields due to the evolution of synoptic patterns (Yang et al., 2021). In 2050, the highest MDA8 ozone concentrations in spring, and summer are under SSP370 scenario, reaching 61.0, and 65.0 ppbv, respectively. Meanwhile, MDA8 ozone in autumn is highest under SSP585 (49.9 ppbv) scenario and in winter is highest under SSP245 (42.1 ppbv) scenario in 2050. By 2050, MDA8 ozone is above the WHO guidelines in spring under four scenarios and in summer under SSP370 and SSP585 scenarios. The changes of MDA8 ozone over 2020–2050 under SSP126 (SSP245) scenario show a slight increase by 0.8 (4.3) ppbv in winter but a large decrease by 5.4 ~13.5 (3.2~11.6) ppbv in the other three seasons. MDA8 ozone concentrations change slightly in four seasons from 2020 to 2050 under SSP370 and SSP585 scenarios, with the differences within 2.9 ppbv.
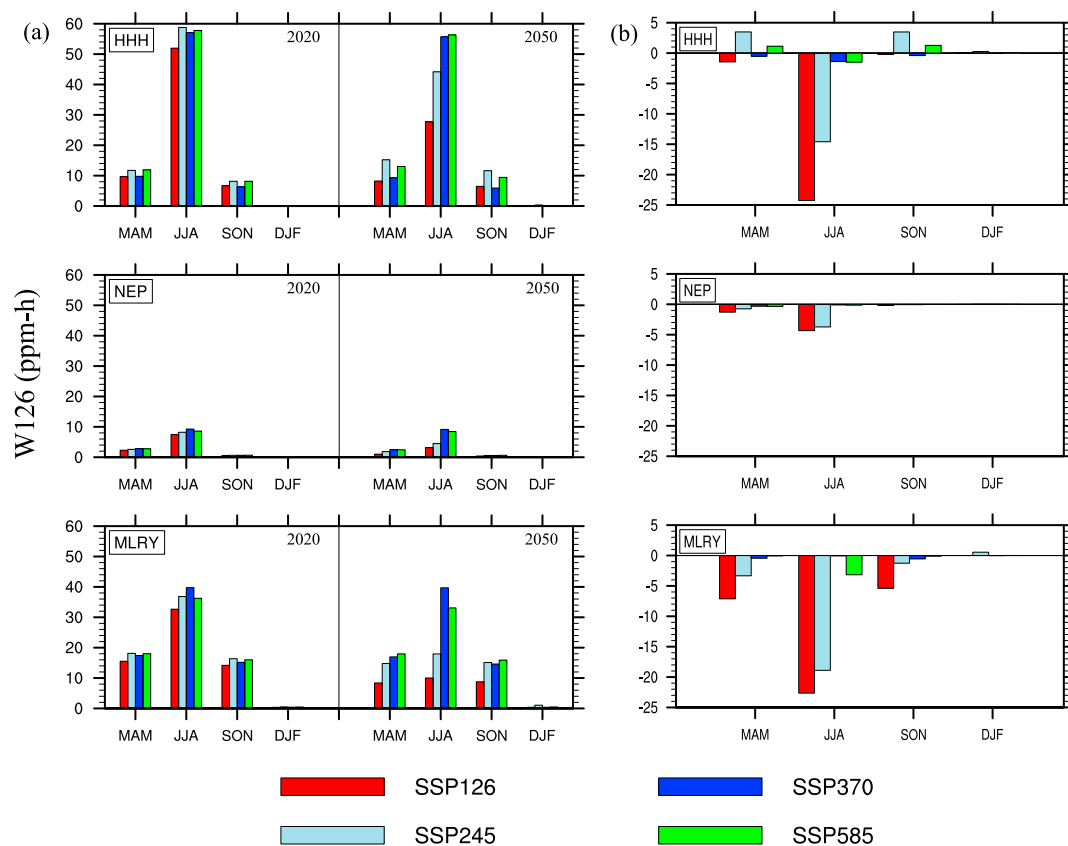
Figure 5. Same as Figure 4, but for seasonal W126.

Seasonal variations of ozone concentrations in NEP in 2020 and 2050 are weak under four scenarios, and seasonal mean MDA8 ozone concentrations are lower than those in the other areas (Figure 4a), which are similar with previous studies reported by Gao et al. (2020), Li et al. (2022), and Kalsoom et al. (2021). In 2020, seasonal mean MDA8 ozone concentrations averaged over the four scenarios are 41.0 ppbv in spring, 42.4 ppbv in summer, 32.3 ppbv in autumn and 24.0 ppbv in winter. Changes of ozone concentrations in autumn and winter are small under four scenarios from 2020 to 2050, only by −1.9 to +1.4 ppbv. For spring and summer, the differences of MDA8 ozone concentrations are large between 2050 and 2020 under SSP126 scenario, with the reductions of 5.7 and 6.6 ppbv. However, ozone concentrations change little under SSP245, SSP370, and SSP585 scenarios in spring and summer, ranging from −4.1 to +0.003 ppbv (Figure 4b). The MDA8 ozone concentrations all satisfy the air quality guideline under four scenarios in 2020 and 2050.

5. W126 (Seasonal Vegetative Ozone Exposure Index) in 2020 and 2050

Figure 5a shows the seasonal W126 under SSP126, SSP245, SSP370, and SSP585 scenarios over three major crop growing areas in 2020 and 2050. Figure 5b shows the difference of seasonal W126 between 2050 and 2020 in three major crop growing areas under four scenarios. As shown in Figure 5a, W126 in the three major crop growing areas is all the highest in summer and the lowest (approaching zero) in winter under four scenarios in 2020 and 2050. Vegetation in the three major crop growing areas suffers from high ozone exposure in summer and is hardly affected by ozone in winter. The seasonal variations of W126 in 2020 and 2050 are largely relative to those of ozone concentrations (Figure 4a), which results from its sigmoidal weighting to ozone levels, that is, emphasizing high ozone concentrations and suppressing low or moderate levels (Lefohn et al., 2018; Lu et al., 2018; Xu et al., 2020).

The seasonal variation characteristics of W126 are quite close over HHH and MLRY. W126 is the highest in summer, followed by spring and autumn and lowest in winter under four scenarios in HHH and MLRY. In HHH (MLRY), W126 under four scenarios in 2020 is in the range of 52.0–58.8 (32.7–39.8) ppm-h in summer, which is

much higher than US three-monthly W126 standard of 21 ppm-h, indicating that ozone is high enough to cause negative effects on plants in summer 2020. Changes of W126 are large in summer by 2050 relative to 2020, especially under SSP126 and SSP245 scenarios. W126 changes slightly under four scenarios in spring, autumn and winter from 2020 to 2050, within the range of −1.5 to +3.5 (−7.1 to +0.5) ppm-h in HHH (MLRY). Compared with other scenarios, W126 in summer 2050 is the highest under SSP585 scenario in HHH and under SSP370 scenario in MLRY, and the lowest under SSP126 scenario in HHH and MLRY. In 2050, W126 in summer is far more than 21 ppm-h under SSP370 and SSP585 scenarios in MLRY and under four scenarios in HHH. The vegetation is more likely to get injured like foliar injury, crop loss due to ozone exposure when W126 exceeds the threshold (EPA, 2015).

Compared with the other two major crop growing areas, seasonal W126 in NEP is lower under four scenarios in 2020 and 2050, showing that the vegetation is likely less affected by ozone exposure. The peak values of W126 under four scenarios appear in summer within the ranges of 7.5–9.3 ppm-h in 2020 and 3.2–9.2 ppm-h in 2050, which are all below US three-monthly W126 standard of 21 ppm-h. W126 in the other seasons is less than 7 ppm-h (0.2–2.8 ppm-h) under four scenarios in 2020 and 2050. W126 changes slightly over 2020–2050 in four seasons under four scenarios, ranging from–4.3 to +0.02 ppm-h. In 2050, SSP370 is the worst scenario for summer W126 in NEP and SSP126 scenario is the best, compared with other scenarios.

6. Health Impact Assessment of Ozone Exposures in 2020 and 2050

Figure 6a shows annual ozone-related deaths (in thousands) from CVD, RD, and COPD for people older than 30 years of age in BTH, YRD, PRD, and SCB in 2020 and 2050 under SSP126, SSP245, SSP370, and SSP585 scenarios. Among the four areas, the change of annual estimated mortality in BTH is more sensitive to ozone change under SSP126, SSP245 and SSP585 scenarios and that in SCB is more sensitive under SSP370 scenarios.

In BTH (YRD), annual estimated mortality is high under SSP245 and SSP585 scenarios in 2020 and the corresponding annual ozone-related deaths from CVD, RD, and COPD reaching 28.1 (18.2) thousand, 23.8 (15.2) thousand and 25.9 (16.4) thousand. From 2020 to 2050, future deaths from CVD, RD, and COPD increase under SSP245 scenario in BTH (YRD) by 4.2 (1.6) thousand, 3.1 (1.1) thousand, and 3.3 (1.2) thousand, respectively, and decrease under SSP126, SSP370, and SSP585 scenarios by 0.9–2.0 (0.7–2.1) thousand, 0.8–1.7 (0.6–1.7) thousand, and 0.9–1.8 (0.7–1.8) thousand, respectively (Figure 6b). The decreased annual ozone-related deaths from CVD, RD, and COPD between 2050 and 2020 are mainly due to the changes of ozone, which is similar with the findings reported by Wang, Hu, et al. (2021) and Chen et al. (2018). The increased ozone-related deaths under SSP245 scenario in BTH (YRD) from 2020 to 2050 may result from an increase in ozone concentrations but a slight reduction in population.

For PRD, annual estimated ozone-related deaths from CVD, RD, and COPD are quite close among four scenarios in 2020, with averaged deaths over four scenarios of 14.1 thousand, 11.6 thousand and 12.5 thousand, respectively. Annual estimated ozone-related deaths in 2020 are similar with the results reported by Zheng et al. (2022). In 2050, the mortality from CVD, RD, and COPD is the highest under SSP585 scenario and lowest under SSP126 scenario, compared with other scenarios. The mortality from CVD, RD, and COPD decreases largely under SSP126 (SSP245) scenario by 2050 relative to 2020 (Figure 6b), reaching 5.3 (2.3) thousand, 4.1 (1.7) thousand and 4.4 (1.7) thousand. Changes of deaths from 2020 to 2050 are slight under SSP370 and SSP585 scenarios for three diseases, within the range of −0.02 to +0.39 thousand. The number of deaths increase slightly under SSP585 scenario by 2050, which mainly results from an increase in population in PRD offsetting a slight reduction in ozone concentrations.

In SCB, annual ozone-related deaths in 2020 are about 18.9 thousand from CVD, 15.6 thousand from RD and 16.8 thousand from COPD averaged over four scenarios, which is little lower than the results studied by Sun et al. (2021). Compared with other scenarios, SSP370 scenario is the worst scenario and SSP126 scenario is the best scenario for the death from CVD, RD, and COPD by 2050. Overall, reductions of population size are larger in this region under four scenarios compared with the other regions from 2020 to 2050. Ozone concentrations decrease under SSP126 and SSP245 scenarios and change slightly under SSP370 and SSP585 scenarios. Therefore, future annual deaths from three diseases show a consistent downward trend from 2020 to 2050, especially under SSP126 scenario (6.0 thousand from CVD, 4.8 thousand from RD and 5.1 thousand from COPD) (Figure 6b). For SSP245, SSP370, and SSP585 scenarios, the reductions of deaths from three diseases over 2020–2050 are ranging from 1.2 to 3.9 thousand.
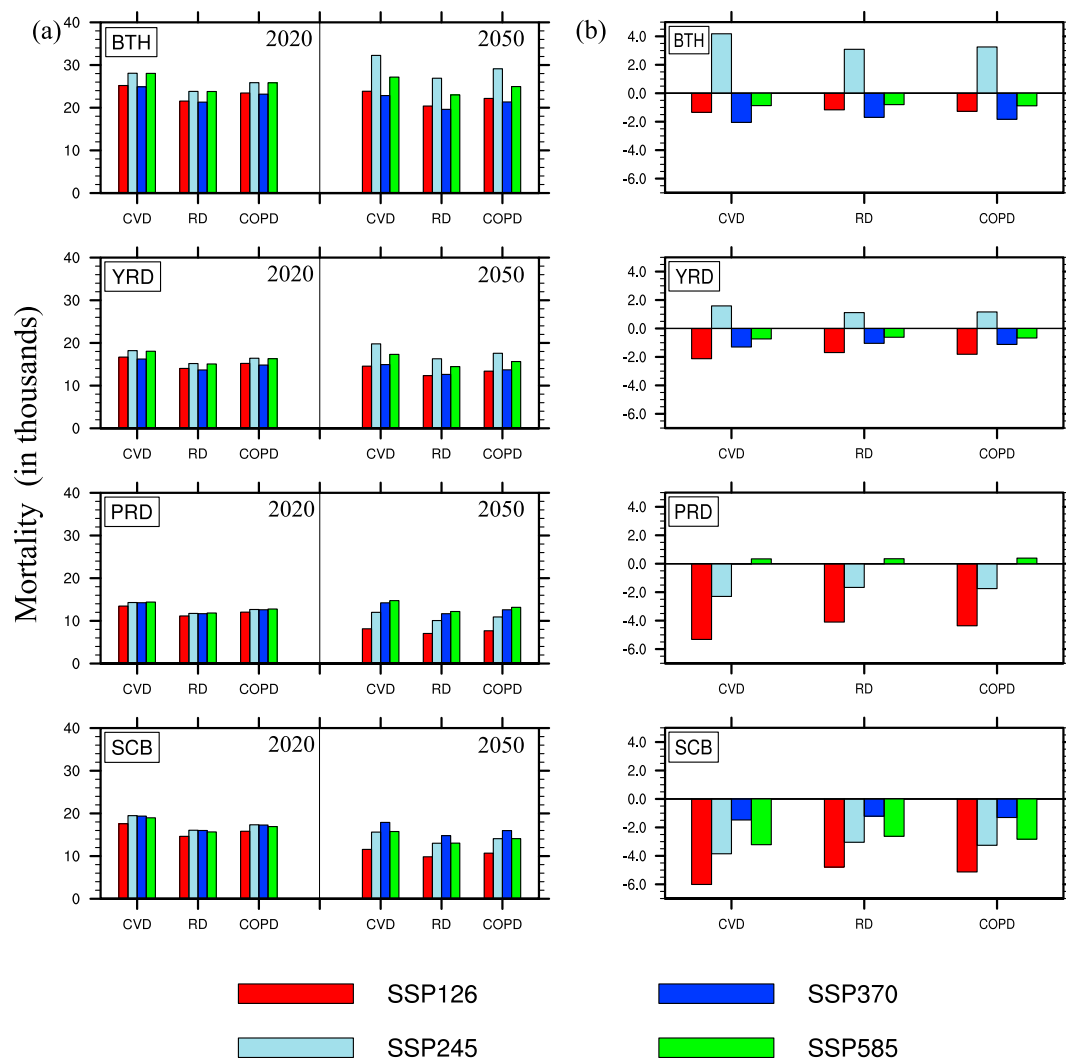
Figure 6. (a) Annual ozone-related deaths (in thousands) in 2020 and 2050 and (b) differences of annual ozone-related deaths (in thousands) between 2050 and 2020 from CVD, RD, and COPD older than 30 in BTH, YRD, PRD, and SCB under SSP126, SSP245, SSP370, and SSP585 scenarios.

7. Conclusions

The present study systematically quantifies effects of ozone on future vegetation and human health in polluted regions and major crop growing areas of China. We use GEOS-Chem to predict the ozone concentrations in 2050 under four different emissions scenarios (SSP126, SSP245, SSP370, and SSP585 scenarios) and then further evaluate the impacts of ozone pollution on future vegetation and premature mortality in four polluted regions and three major crop growing areas of China. Model can capture the spatiotemporal distributions of the observed ozone concentrations in China in 2020, with r of 0.76, 0.77, 0.74 and 0.77 under SSP126, SSP245, SSP370, and SSP585 scenarios, respectively.

MDA8 ozone concentrations in BTH, YRD, HHH and MLRY are all highest in summer and lowest in winter in 2020 and 2050, reaching 62.6–76.9 ppbv, 51.7–67.7 ppbv, 63.7–79.2 ppbv and 51.3–70.8 ppbv, respectively, under four scenarios in summer 2050. The seasonal variation of MDA8 ozone in PRD (SCB and NEP) is high in spring and autumn (spring and summer) and low in summer and winter (autumn and winter) in 2020 and 2050. Generally, ozone concentrations under SSP126 scenario are the lowest in all regions in 2050 and those under SSP370 scenario are the highest in summer. By 2050, seasonal MDA8 ozone changes much (−15.5 to +11.9 ppbv) under SSP126 and SSP245 scenarios in all regions due to large changes of emissions relative to

2020, especially in summer. Ozone pollution is relatively severe in BTH, YRD, HHH, and MLRY, which is all above the WHO air quality guidelines in summer 2050 under four scenarios.

The seasonal variations of W126 under all scenarios in 2020 and 2050 are similar to the corresponding variations of ozone concentrations, but with larger differences between four seasons due to sigmoidal weighting to ozone levels. W126 in HHH and MLRY is highest in summer and approaching zero in winter in 2020 and 2050, which indicates that vegetation in these regions is at high risk in summer and virtually unaffected by ozone exposure in winter. For NEP, W126 is below the maximum of US secondary standard (21 ppm-h) in four seasons in 2020 and 2050 due to low ozone concentrations. In these three regions, W126 will change greatly under SSP126 and SSP245 scenarios and change little under SSP585 and SSP370 scenarios from 2020 to 2050. By 2050, W126 in summer is far more than 21 ppm-h under SSP370 and SSP585 scenarios in MLRY and under four scenarios in HHH.

We use mortality to quantify impacts of ozone pollution on human health in China in 2020 and 2050. The largest number of future deaths from CVD, RD, and COPD in 2050 is projected under SSP245 scenario in BTH and YRD. The increased ozone-related deaths under SSP245 scenario in BTH (YRD) from 2020 to 2050 may result from an increase in ozone concentrations but a slight reduction in population. In 2050, SSP370 (SSP585) scenario is the worst scenario in SCB (PRD) compared with other scenarios for the death from CVD, RD, and COPD. The mortality from CVD, RD, and COPD in PRD decreases largely under SSP126 and SSP245 scenarios and changes slightly under SSP370 and SSP585 scenarios by 2050 relative to 2020. Future annual deaths from three diseases show a consistent downward trend in SCB from 2020 to 2050 owing to reductions in population and slight changes in ozone concentrations, especially under SSP126 scenario.

Our predictions of future ozone concentrations and their impacts on vegetation and human health are important to implement control measures of air pollution and protection schemes of human health and vegetation. The uncertainties in this study may from model resolutions, chemical mechanisms, meteorology and future emissions scenarios. We will take into account the influence of climate changes in future studies, as which is an important factor to changes of future ozone concentrations.

Data Availability Statement

Gridded population data in 2020 and 2050 under four SSPs scenarios is from http://sedac.ciesin.columbia.edu/data/set/popdynamics-1-8th-pop-base-year-projection-ssp-2000-2100-rev01/data-download (Jones & O'Neill, 2020). The percentage of population over 30 years old is achieved from the United Nations estimates (https://population.un.org/wpp/Download/Standard/Population/) (United Nations, 2019). The baseline mortality of the particular disease category is obtained from Global Health Estimates 2019 by World Health Organization (https://www.who.int/data/global-health-estimates) (WHO, 2020). Hourly ozone observations are available from the China National Environmental Monitoring Center (https://quotsoft.net/air/) (CNEMC, 2023). The GEOS-Chem model (v12-09) is available at https://wiki.seas.harvard.edu/geos-chem/index.php/GEOS-Chem_12#12.9.2 (The International GEOS-Chem User Community, 2020). Global anthropogenic emissions and open-burning emissions of the SSPs scenarios can be downloaded at https://esgf-node.llnl.gov/search/input4MIPs/ (Gidden et al., 2019). NCAR Command Language (NCL) version 6.6.2 is used for figures (The NCAR Command Language, 2019).

References

Alexis, N. E., & Carlsten, C. (2014). Interplay of air pollution and asthma immunopathogenesis: A focused review of diesel exhaust and ozone. *International Immunopharmacology*, *23*(1), 347–355. https://doi.org/10.1016/j.intimp.2014.08.009

Amos, H. M., Jacob, D. J., Holmes, C. D., Fisher, J. A., Wang, Q., Yantosca, R. M., et al. (2012). Gas-particle partitioning of atmospheric Hg(II) and its effect on global mercury deposition. *Atmospheric Chemistry and Physics*, *12*(1), 591–603. https://doi.org/10.5194/acp-12-591-2012

Bhatia, A., Tomer, R., Kumar, V., Singh, S., & Pathak, D. S. (2012). Impact of tropospheric ozone on crop growth and productivity – A review. *Journal of Scientific and Industrial Research*, *71*(2), 97–112. http://nopr.niscpr.res.in/handle/123456789/13486

Bian, H., & Prather, M. J. (2002). Fast-J2: Accurate simulation of stratospheric photolysis in global chemical models. *Journal of Atmospheric Chemistry*, *41*(3), 281–296. https://doi.org/10.1023/A:1014980619462

Boylan, J. W., & Russell, A. G. (2006). PM and light extinction model performance metrics, goals, and criteria for three-dimensional air quality models. *Atmospheric Environment*, *40*(26), 4946–4959. https://doi.org/10.1016/j.atmosenv.2005.09.087

Cao, Y., Qiao, X., Hopke, P. K., Ying, Q., Zhang, Y., Zeng, Y., et al. (2020). Ozone pollution in the west China rain zone and its adjacent regions, Southwestern China: Concentrations, ecological risk, and sources. *Chemosphere*, *256*, 127008. https://doi.org/10.1016/j.chemosphere.2020.127008

Chen, K., Fiore, A. M., Chen, R., Jiang, L., Jones, B., Schneider, A., et al. (2018). Future ozone-related acute excess mortality under climate and population change scenarios in China: A modeling study. *PLoS Medicine*, *15*(7), e1002598. https://doi.org/10.1371/journal.pmed.1002598

CNEMC. (2023). China National Environmental Monitoring Center: Surface O_3 measurements. [Dataset]. Retrieved from https://quotsoft.net/air/

Cohen, A. J., Brauer, M., Burnett, R., Anderson, H. R., Frostad, J., Estep, K., et al. (2017). Estimates and 25-year trends of the global burden of disease attributable to ambient air pollution: An analysis of data from the Global Burden of Diseases Study 2015. *Lancet*, *389*(10082), 1907–1918. https://doi.org/10.1016/S0140-6736(17)30505-6

Dang, R., & Liao, H. (2019). Radiative forcing and health impact of aerosols and ozone in China as the consequence of Clean Air Actions over 2012–2017. *Geophysical Research Letters*, *46*(21), 12511–12519. https://doi.org/10.1029/2019gl084605

Dang, R., Liao, H., & Fu, Y. (2021). Quantifying the anthropogenic and meteorological influences on summertime surface ozone in China over 2012–2017. *Science of the Total Environment*, *754*, 142394. https://doi.org/10.1016/j.scitotenv.2020.142394

Emberson, L. (2020). Effects of ozone on agriculture, forests and grasslands. *Philosophical Transactions of the Royal Society A-Mathematical, Physical & Engineering Sciences*, *378*(2183), 20190327. https://doi.org/10.1098/rsta.2019.0327

Feng, Z., Hu, E., Wang, X., Jiang, L., & Liu, X. (2015). Ground-level O_3 pollution and its impacts on food crops in China: A review. *Environmental Pollution*, *199*, 42–48. https://doi.org/10.1016/j.envpol.2015.01.016

Gao, C., Xiu, A., Zhang, X., Chen, W., Liu, Y., Zhao, H., & Zhang, S. (2020). Spatiotemporal characteristics of ozone pollution and policy implications in Northeast China. *Atmospheric Pollution Research*, *11*(2), 357–369. https://doi.org/10.1016/j.apr.2019.11.008

Gidden, M. J., Riahi, K., Smith, S. J., Fujimori, S., Luderer, G., Kriegler, E., et al. (2019). Global emissions pathways under different socio-economic scenarios for use in CMIP6: A dataset of harmonized emissions trajectories through the end of the century. *Geoscientific Model Development*, *12*(4), 1443–1475. https://doi.org/10.5194/gmd-12-1443-2019

Goodman, J. E., Prueitt, R. L., Sax, S. N., Pizzurro, D. M., Lynch, H. N., Zu, K., & Venditti, F. J. (2015). Ozone exposure and systemic bio-markers: Evaluation of evidence for adverse cardiovascular health impacts. *Critical Reviews in Toxicology*, *45*(5), 412–452. https://doi.org/10.3109/10408444.2015.1031371

Grulke, N. E., & Heath, R. L. (2019). Ozone effects on plants in natural ecosystems. *Plant Biology*, *22*(Suppl 1), 12–37. https://doi.org/10.1111/plb.12971

Guenther, A. B., Jiang, X., Heald, C. L., Sakulyanontvittaya, T., Duhl, T., Emmons, L. K., & Wang, X. (2012). The Model of Emissions of Gases and Aerosols from Nature version 2.1 (MEGAN2.1): An extended and updated framework for modeling biogenic emissions. *Geoscientific Model Development*, *5*(6), 1471–1492. https://doi.org/10.5194/gmd-5-1471-2012

Hollaway, M. J., Arnold, S. R., Collins, W. J., Folberth, G., & Rap, A. (2017). Sensitivity of midnineteenth century tropospheric ozone to atmospheric chemistry-vegetation interactions. *Journal of Geophysical Research: Atmospheres*, *122*(4), 2452–2473. https://doi.org/10.1002/2016JD025462

Holmes, C. D., Bertram, T. H., Confer, K. L., Graham, K. A., Ronan, A. C., Wirks, C. K., & Shah, V. (2019). The role of clouds in the tropospheric NOx cycle: A new modeling approach for cloud chemistry and its global implications. *Geophysical Research Letters*, *46*(9), 4980–4990. https://doi.org/10.1029/2019GL081990

Hong, C., Zhang, Q., Zhang, Y., Davis, S. J., Tong, D., Zheng, Y., et al. (2019). Impacts of climate change on future air quality and human health in China. *Proceedings of the National Academy of Sciences of the United States of America*, *116*(35), 17193–17200. https://doi.org/10.1073/pnas.1812881116

Hu, M., Wang, Y., Wang, S., Jiao, M., Huang, G., & Xia, B. (2021). Spatial-temporal heterogeneity of air pollution and its relationship with meteorological factors in the Pearl River Delta, China. *Atmospheric Environment*, *254*, 118415. https://doi.org/10.1016/j.atmosenv.2021.118415

Jerrett, M., Burnett, R. T., Pope, C. A., 3rd, Ito, K., Thurston, G., Krewski, D., et al. (2009). Long-term ozone exposure and mortality. *New England Journal of Medicine*, *360*(11), 1085–1095. https://doi.org/10.1056/NEJMoa0803894

Jones, B., & O'Neill, B. C. (2020). Global one-eighth degree population base year and projection grids based on the Shared Socioeconomic Pathways, Revision 01. [Dataset]. Retrieved from https://doi.org/10.7927/m30p-j498

Kalsoom, U., Wang, T., Ma, C., Shu, L., Huang, C., & Gao, L. (2021). Quadrennial variability and trends of surface ozone across China during 2015–2018: A regional approach. *Atmospheric Environment*, *245*, 117989. https://doi.org/10.1016/j.atmosenv.2020.117989

Knote, C., Tuccella, P., Curci, G., Emmons, L., Orlando, J. J., Madronich, S., et al. (2015). Influence of the choice of gas-phase mechanism on predictions of key gaseous pollutants during the AQMEII phase-2 intercomparison. *Atmospheric Environment*, *115*, 553–568. https://doi.org/10.1016/j.atmosenv.2014.11.066

Lapina, K., Henze, D. K., Milford, J. B., Huang, M., Lin, M., Fiore, A. M., et al. (2014). Assessment of source contributions to seasonal vegetative exposure to ozone in the U.S. *Journal of Geophysical Research: Atmospheres*, *119*(1), 324–340. https://doi.org/10.1002/2013jd020905

Lefohn, A. S., Malley, C. S., Smith, L., Wells, B., Hazucha, M., Simon, H., et al. (2018). Tropospheric ozone assessment report: Global ozone metrics for climate change, human health, and crop/ecosystem research. *Elementa: Science of the Anthropocene*, *6*, 27. https://doi.org/10.1525/elementa.279

Li, L.-G., Liu, N., Shen, L., Zhao, Z., Wang, H., Wang, Y., et al. (2022). Ozone concentration at various heights near the surface layer in Shenyang, Northeast China. *Frontiers in Environmental Science*, *10*. https://doi.org/10.3389/fenvs.2022.1011508

Li, P., De Marco, A., Feng, Z., Anav, A., Zhou, D., & Paoletti, E. (2018). Nationwide ground-level ozone measurements in China suggest serious risks to forests. *Environmental Pollution*, *237*, 803–813. https://doi.org/10.1016/j.envpol.2017.11.002

Lin, J.-T., & McElroy, M. B. (2010). Impacts of boundary layer mixing on pollutant vertical profiles in the lower troposphere: Implications to satellite remote sensing. *Atmospheric Environment*, *44*(14), 1726–1739. https://doi.org/10.1016/j.atmosenv.2010.02.009

Liu, H., Jacob, D. J., Bey, I., & Yantosca, R. M. (2001). Constraints from ^{210}Pb and ^{7}Be on wet deposition and transport in a global three-dimensional chemical tracer model driven by assimilated meteorological fields. *Journal of Geophysical Research: Atmospheres*, *106*(D11), 12109–12128. https://doi.org/10.1029/2000JD900839

Liu, S., Xing, J., Wang, S., Ding, D., Cui, Y., & Hao, J. (2021). Health benefits of emission reduction under 1.5 degrees C pathways far outweigh climate-related variations in China. *Environmental Science and Technology*, *55*(16), 10957–10966. https://doi.org/10.1021/acs.est.1c01583

Liu, Z., Doherty, R. M., Wild, O., O'Connor, F. M., & Turnock, S. T. (2022). Tropospheric ozone changes and ozone sensitivity from the present day to the future under Shared Socio-economic Pathways. *Atmospheric Chemistry and Physics*, *22*(2), 1209–1227. https://doi.org/10.5194/acp-22-1209-2022

Lou, S., Liao, H., Yang, Y., & Mu, Q. (2015). Simulation of the interannual variations of tropospheric ozone over China: Roles of variations in meteorological parameters and anthropogenic emissions. *Atmospheric Environment*, *122*, 839–851. https://doi.org/10.1016/j.atmosenv.2015.08.081

Lu, X., Hong, J., Zhang, L., Cooper, O. R., Schultz, M. G., Xu, X., et al. (2018). Severe surface ozone pollution in China: A global perspective. *Environmental Science and Technology Letters*, *5*(8), 487–494. https://doi.org/10.1021/acs.estlett.8b00366

Lu, X., Zhang, L., Chen, Y., Zhou, M., Zheng, B., Li, K., et al. (2019). Exploring 2016–2017 surface ozone pollution over China: Source contributions and meteorological influences. *Atmospheric Chemistry and Physics*, *19*(12), 8339–8361. https://doi.org/10.5194/acp-19-8339-2019

Lu, X., Zhang, L., Wang, X., Gao, M., Li, K., Zhang, Y., et al. (2020). Rapid increases in warm-season surface ozone and resulting health impact in China since 2013. *Environmental Science and Technology Letters*, *7*(4), 240–247. https://doi.org/10.1021/acs.estlett.0c00171

Malley, C. S., Henze, D. K., Kuylenstierna, J. C. I., Vallack, H. W., Davila, Y., Anenberg, S. C., et al. (2017). Updated global estimates of respiratory mortality in adults >/=30 years of age attributable to long-term ozone exposure. *Environmental Health Perspectives*, *125*(8), 087021. https://doi.org/10.1289/EHP1390

Mar, K. A., Ojha, N., Pozzer, A., & Butler, T. M. (2016). Ozone air quality simulations with WRF-Chem (v3.5.1) over Europe: Model evaluation and chemical mechanism comparison. *Geoscientific Model Development*, *9*(10), 3699–3728. https://doi.org/10.5194/gmd-9-3699-2016

Marco, A. D., Anav, A., Sicard, P., Feng, Z., & Paoletti, E. (2020). High spatial resolution ozone risk-assessment for Asian forests. *Environmental Research Letters*, *15*(10), 104095. https://doi.org/10.1088/1748-9326/abb501

McDuffie, E. E., Fibiger, D. L., Dubé, W. P., Lopez Hilfiker, F., Lee, B. H., Jaeglé, L., et al. (2018). ClNO$_2$ yields from aircraft measurements during the 2015 WINTER Campaign and critical evaluation of the current parameterization. *Journal of Geophysical Research: Atmospheres*, *123*(22), 12994–913015. https://doi.org/10.1029/2018JD029358

Mousavinezhad, S., Choi, Y., Pouyaei, A., Ghahremanloo, M., & Nelson, D. L. (2021). A comprehensive investigation of surface ozone pollution in China, 2015–2019: Separating the contributions from meteorology and precursor emissions. *Atmospheric Research*, *257*, 105599. https://doi.org/10.1016/j.atmosres.2021.105599

Murray, L. T., Jacob, D. J., Logan, J. A., Hudman, R. C., & Koshak, W. J. (2012). Optimized regional and interannual variability of lightning in a global chemical transport model constrained by LIS/OTD satellite data. *Journal of Geophysical Research: Atmospheres*, *117*(D20). https://doi.org/10.1029/2012JD017934

Ni, R., Lin, J., Yan, Y., & Lin, W. (2018). Foreign and domestic contributions to springtime ozone over China. *Atmospheric Chemistry and Physics*, *18*(15), 11447–11469. https://doi.org/10.5194/acp-18-11447-2018

O'Neill, B. C., Kriegler, E., Ebi, K. L., Kemp-Benedict, E., Riahi, K., Rothman, D. S., et al. (2017). The roads ahead: Narratives for Shared Socioeconomic Pathways describing world futures in the 21st century. *Global Environmental Change*, *42*, 169–180. https://doi.org/10.1016/j.gloenvcha.2015.01.004

O'Neill, B. C., Tebaldi, C., van Vuuren, D. P., Eyring, V., Friedlingstein, P., Hurtt, G., et al. (2016). The Scenario Model Intercomparison Project (ScenarioMIP) for CMIP6. *Geoscientific Model Development*, *9*(9), 3461–3482. https://doi.org/10.5194/gmd-9-3461-2016

Qiao, X., Wang, P., Zhang, J., Zhang, H., Tang, Y., Hu, J., & Ying, Q. (2019). Spatial-temporal variations and source contributions to forest ozone exposure in China. *Science of the Total Environment*, *674*, 189–199. https://doi.org/10.1016/j.scitotenv.2019.04.106

Ren, W., Tian, H., Chen, G., Liu, M., Zhang, C., Chappelka, A. H., & Pan, S. (2007). Influence of ozone pollution and climate variability on net primary productivity and carbon storage in China's grassland ecosystems from 1961 to 2000. *Environmental Pollution*, *149*(3), 327–335. https://doi.org/10.1016/j.envpol.2007.05.029

Ren, W., Tian, H., Liu, M., Zhang, C., Chen, G., Pan, S., et al. (2007). Effects of tropospheric ozone pollution on net primary productivity and carbon storage in terrestrial ecosystems of China. *Journal of Geophysical Research*, *112*(D22). https://doi.org/10.1029/2007jd008521

Ren, W., Tian, H., Tao, B., Chappelka, A., Sun, G., Lu, C., et al. (2011). Impacts of tropospheric ozone and climate change on net primary productivity and net carbon exchange of China's forest ecosystems. *Global Ecology and Biogeography*, *20*(3), 391–406. https://doi.org/10.1111/j.1466-8238.2010.00606.x

Sander, S. P., Abbatt, J. J., Barker, R., Burkholder, J. B., Friedl, R. R., Golden, D. M., et al. (2011). *Chemical kinetics and photochemical data for use in atmospheric studies*. Evaluation No. 17. JPL Publication 10-6, Jet Propulsion Laboratory. Retrieved from http://jpldataeval.jpl.nasa.gov

Sauvage, B., Martin, R. V., van Donkelaar, A., Liu, X., Chance, K., Jaeglé, L., et al. (2007). Remote sensed and in situ constraints on processes affecting tropical tropospheric ozone. *Atmospheric Chemistry and Physics*, *7*(3), 815–838. https://doi.org/10.5194/acp-7-815-2007

Sousa, S. I., Alvim-Ferraz, M. C., & Martins, F. G. (2013). Health effects of ozone focusing on childhood asthma: What is now known–A review from an epidemiological point of view. *Chemosphere*, *90*(7), 2051–2058. https://doi.org/10.1016/j.chemosphere.2012.10.063

Sun, Y., Yin, H., Lu, X., Notholt, J., Palm, M., Liu, C., et al. (2021). The drivers and health risks of unexpected surface ozone enhancements over the Sichuan Basin, China, in 2020. *Atmospheric Chemistry and Physics*, *21*(24), 18589–18608. https://doi.org/10.5194/acp-21-18589-2021

Tai, A. P. K., Martin, M. V., & Heald, C. L. (2014). Threat to future global food security from climate change and ozone air pollution. *Nature Climate Change*, *4*(9), 817–821. https://doi.org/10.1038/nclimate2317

Tai, A. P. K., & Val Martin, M. (2017). Impacts of ozone air pollution and temperature extremes on crop yields: Spatial variability, adaptation and implications for future food security. *Atmospheric Environment*, *169*, 11–21. https://doi.org/10.1016/j.atmosenv.2017.09.002

The International GEOS-Chem User Community. (2020). geoschem/geos-chem: GEOS-Chem 12.9.2 (12.9.2) [Software]. Zenodo. https://doi.org/10.5281/zenodo.3959279

The NCAR Command Language. (2019). The NCAR Command Language (Version 6.6.2). [Software]. Boulder, Colorado: UCAR/NCAR/CISL/TDD. https://doi.org/10.5065/D6WD3XH5

Turner, M. C., Jerrett, M., Pope, C. A., 3rd, Krewski, D., Gapstur, S. M., Diver, W. R., et al. (2016). Long-term ozone exposure and mortality in a large prospective study. *American Journal of Respiratory and Critical Care Medicine*, *193*(10), 1134–1142. https://doi.org/10.1164/rccm.201508-1633OC

Uddling, J., Hogg, A. J., Teclaw, R. M., Carroll, M. A., & Ellsworth, D. S. (2010). Stomatal uptake of O$_3$ in aspen and aspen-birch forests under free-air CO$_2$ and O$_3$ enrichment. *Environmental Pollution*, *158*(6), 2023–2031. https://doi.org/10.1016/j.envpol.2009.12.001

United Nations, Department of Economic and Social Affairs, Population Division. (2019). World Population Prospects 2019, Online Edition. Rev. 1. [Dataset]. Retrieved from: https://population.un.org/wpp/Download/Standard/Population/

U.S. Environmental Protection Agency. (2015). National ambient air quality standards for ozone; Final rule, 80 Fed. Reg. 65292. Retrieved from https://www.federalregister.gov/d/2015-26594

Wang, L., Xing, L., Wu, X., Sun, J., & Kong, M. (2020). Spatiotemporal variations and risk assessment of ambient air O$_3$, PM$_{10}$ and PM$_{2.5}$ in a coastal city of China. *Ecotoxicology*, *30*(7), 1333–1342. https://doi.org/10.1007/s10646-020-02295-0

Wang, T., Wei, X. L., Ding, A. J., Poon, C. N., Lam, K. S., Li, Y. S., et al. (2009). Increasing surface ozone concentrations in the background atmosphere of Southern China, 1994–2007. *Atmospheric Chemistry and Physics*, *9*(16), 6217–6227. https://doi.org/10.5194/acp-9-6217-2009

Wang, T., Xue, L., Brimblecombe, P., Lam, Y. F., Li, L., & Zhang, L. (2017). Ozone pollution in China: A review of concentrations, meteorological influences, chemical precursors, and effects. *Science of the Total Environment*, *575*, 1582–1596. https://doi.org/10.1016/j.scitotenv.2016.10.081

Wang, Y., Hu, J., Zhu, J., Li, J., Qin, M., Liao, H., et al. (2021). Health Burden and economic impacts attributed to PM$_{2.5}$ and O$_3$ in China from 2010 to 2050 under different Representative Concentration Pathway scenarios. *Resources, Conservation and Recycling*, *173*, 105731. https://doi.org/10.1016/j.resconrec.2021.105731

Wang, Y., Jacob, D. J., & Logan, J. A. (1998). Global simulation of tropospheric O$_3$-NOx-hydrocarbon chemistry: 3. Origin of tropospheric ozone and effects of nonmethane hydrocarbons. *Journal of Geophysical Research*, *103*(D9), 10757–10767. https://doi.org/10.1029/98JD00156

Wang, Y., Shen, J., Wang, H., Wu, G., Chen, Y., Liu, T., et al. (2021). Unexpected seasonal variations and high levels of ozone observed at the summit of Nanling Mountains: Impact of Asian monsoon on southern China. *Atmospheric Environment*, *253*, 118378. https://doi.org/10.1016/j.atmosenv.2021.118378

Weng, X., Li, J. W., Forster, G. L., & Nowack, P. (2023). Large modeling uncertainty in projecting decadal surface ozone changes over city clusters of China. *Geophysical Research Letters*, *50*(9). https://doi.org/10.1029/2023GL103241

Wesely, M. L. (1989). Parameterization of surface resistances to gaseous dry deposition in regional-scale numerical models. *Atmospheric Environment*, *23*(6), 1293–1304. https://doi.org/10.1016/0004-6981(89)90153-4

World Health Organization. (2020). Global Health Estimates 2019: Deaths by cause, age, sex, by country and by region, 2000-2019. [Dataset]. Geneva. Retrieved from: https://www.who.int/data/global-health-estimates

Xia, L., Zhao, F., Mao, K., Yuan, Z., Zuo, Z., & Xu, T. (2018). SPI-based analyses of drought changes over the past 60 years in China's major crop-growing areas. *Remote Sensing*, *10*(2), 171. https://doi.org/10.3390/rs10020171

Xu, B., Wang, T., Ma, D., Song, R., Zhang, M., Gao, L., et al. (2022). Impacts of regional emission reduction and global climate change on air quality and temperature to attain carbon neutrality in China. *Atmospheric Research*, *279*, 106384. https://doi.org/10.1016/j.atmosres.2022.106384

Xu, X., Lin, W., Xu, W., Jin, J., Wang, Y., Zhang, G., et al. (2020). Long-term changes of regional ozone in China: Implications for human health and ecosystem impacts. *Elementa: Science of the Anthropocene*, *8*, 13. https://doi.org/10.1525/elementa.409

Yang, X., Wu, K., Wang, H., Liu, Y., Gu, S., Lu, Y., et al. (2020). Summertime ozone pollution in Sichuan Basin, China: Meteorological conditions, sources and process analysis. *Atmospheric Environment*, *226*, 117392. https://doi.org/10.1016/j.atmosenv.2020.117392

Yang, X. Y., Wu, K., Lu, Y. Q., Wang, S. G., Qiao, Y. H., Zhang, X. L., et al. (2021). Origin of regional springtime ozone episodes in the Sichuan Basin, China: Role of synoptic forcing and regional transport. *Environmental Pollution*, *278*, 116845. https://doi.org/10.1016/j.envpol.2021.116845

Yienger, J. J., & Levy Ii, H. (1995). Empirical model of global soil-biogenic NOχ emissions. *Journal of Geophysical Research: Atmospheres*, *100*(D6), 11447–11464. https://doi.org/10.1029/95JD00370

Zhang, L., Gong, S., Padro, J., & Barrie, L. (2001). A size-segregated particle dry deposition scheme for an atmospheric aerosol module. *Atmospheric Environment*, *35*(3), 549–560. https://doi.org/10.1016/S1352-2310(00)00326-5

Zhao, H., Wang, L., Zhang, Z., Qi, Q., & Zhang, H. (2022). Quantifying ecological and health risks of ground-level O$_3$ across China during the implementation of the Three-year Action Plan for cleaner air. *Science of the Total Environment*, *817*, 153011. https://doi.org/10.1016/j.scitotenv.2022.153011

Zheng, D. Y., Huang, X. J., & Guo, Y. H. (2022). Spatiotemporal variation of ozone pollution and health effects in China. *Environmental Science and Pollution Research*, *29*(38), 57808–57822. https://doi.org/10.1007/s11356-022-19935-z

Zheng, J., Zhong, L., Wang, T., Louie, P. K. K., & Li, Z. (2010). Ground-level ozone in the Pearl River Delta region: Analysis of data from a recently established regional air quality monitoring network. *Atmospheric Environment*, *44*(6), 814–823. https://doi.org/10.1016/j.atmosenv.2009.11.032

Zhu, J., & Liao, H. (2016). Future ozone air quality and radiative forcing over China owing to future changes in emissions under the Representative Concentration Pathways (RCPs). *Journal of Geophysical Research: Atmospheres*, *121*(4), 1978–2001. https://doi.org/10.1002/2015jd023926

Zhu, J., Liao, H., Mao, Y., Yang, Y., & Jiang, H. (2017). Interannual variation, decadal trend, and future change in ozone outflow from East Asia. *Atmospheric Chemistry and Physics*, *17*(5), 3729–3747. https://doi.org/10.5194/acp-17-3729-2017